Structure-Based Rational Screening of Novel Hit Compounds with Structural Diversity for Cytochrome P450 Sterol 14α-Demethylase from *Penicillium digitatum*

Qingye Zhang,[§,†,‡] Ding Li,[§,†] Pei Wei,[†] Jie Zhang,[†] Jian Wan,*[,†] Yangliang Ren,[†] Zhigang Chen,[†] Deli Liu,[†] Ziniu Yu,[†,‡] and Lingling Feng*[,†]

Key Laboratory of Pesticide & Chemical Biology (CCNU), Ministry of Education; College of Chemistry, Central China Normal University, Wuhan 430079, P R China, and State Key Laboratory for Agricultural Microbiology, National Engineering Research Centre of Microbial Pesticides, Huazhong Agricultural University, Wuhan 430070, P R China

Received November 1, 2009

Cytochrome P450 sterol 14α-demethylases (CYP51s) are essential enzymes in sterol biosynthesis and well-known as the target of antifungal drugs. All fungal CYP51s are integral membrane proteins, making structural and biophysical characterization more challenging. The X-ray crystallographic structure of CYP51 isolated from *Mycobacterium tuberculosis* (MT-CYP51) is the unique reported one hitherto. In the present study, a homology modeling three-dimensional structure of CYP51 from *Penicillium digitatum* (PD-CYP51) was generated by CPHmodels, in which the accuracy of sequence alignment could be improved by taking into account further structural conservation information, using MT-CYP51 as the template. Interaction mechanism between the active site of PD-CYP51 and its inhibitors were further investigated by molecular dynamics simulating and molecular docking. With the effective docking process and interaction analysis information, structure-based virtual screening was performed to pick out the thirty new potential inhibiting compounds with structural diversity by using a new virtual screening strategy including Flex-Pharm/PMF/GOLD//FlexX/PMF/GOLD molecular docking procedures, and finally, seven new hit compounds out of SPECs database with potent inhibitory ability were validated by bioaffinity assays at enzyme level and on *P. digitatum* in vitro. The positive results indicated that all modeling strategies and screening processes presented in the current study most like to be an encouraging way in search of novel lead compounds with structural diversity for the specifically individual fungal CYP51s of both plants and human pathogens in the future.

INTRODUCTION

Sterol 14α-demethylase (CYP51) belongs to a cytochrome P450 family and is the only family of P450 superfamily which is widely distributed in different biological kingdoms and serves the same function.[1,2] In all cases, it catalyzes removal of a methyl group at position C14 in the sterol molecule.[3,4] This is a key step in cholesterol, ergosterol, and phytosterol synthesis in animals, fungi, and plants, respectively. Because CYP51s play a key role in fungal sterol biosynthetic pathways, they have been important targets for antifungal inhibitor design,[5] such as CYP51s from *Candida albicans* (CA),[6−8] *Mycobacterium tuberculosis* (MT),[9−12] *Magnaporthe grisea* (MG),[13] and *Penicillium digitatum* (PD).[14] Especially CYP51s from *Candida albicans* and *Mycobacterium tuberculosis* were the object of many studies attempting to develop new various antibiotics or fungicides, and some positive results have been achieved.[15−18]

Azoles have been found as one category of successful broad spectrum sterol 14α-demethylase inhibitors (DMIs),[6−12,19] which have been the lead agents for the control fungal diseases of plants, human and animals for over three decades.[20] Miconazole,[21] oxiconazole,[22] and ketoconazole[23] are the examples of commercial potent antibiotics for human's fungal disease treatment, and tricyclazole,[24] triadimefon,[25] and diniconazole[26] are example for plants. Azoles fungicides inhibit the synthesis of ergosterol, the bulk sterol in fungal membranes, by binding to the heme cofactor located in the active site of fungal CYP51. The inhibition of CYP51 causes accumulation of methylated sterol, depletion of ergosterol, and therefore hinders cytoplasmic membrane synthesis and growth of fungi.[19]

Decreased sensitivity and field resistance to certain DMIs, however, have been reported in at least thirteen species of pathogens.[27] Molecular mechanisms leading to the DMIs resistance have been studied intensively[28] in the plants and human pathogens. The major mechanisms include (i) overexpression of the CYP51 gene, resulting in increasing production of the CYP51 target protein,[29,30] (ii) point mutations in the CYP51 target protein, leading to a decreased affinity of DMIs to the target protein,[31,32] and (iii) reduced accumulation of DMIs in fungal cells through up-regulation of active efflux proteins. In human and plants pathogens, particularly *Candida albicans* and *Magnaporthe grisea*, point mutations in the CYP51 target protein were shown as the primary determinants of azole resistance.[20] Resistance to azoles is an emerging major challenge in controlling fungal pathogens of plants and human at present.

* To whom correspondence should be addressed. Phone: +86-27-67862022. Fax: +86-27-67862022. E-mail: jianwan@mail.ccnu.edu.cn (J.W.); fll708@mail.ccnu.edu.cn (L.F.).
† Central China Normal University.
‡ Huazhong Agricultural University.
§ These authors contributed equally to this study.

10.1021/ci900425t
Published on Web 01/20/2010

Green mold of citrus, caused by *Penicillium digitatum*, is the major postharvest disease of grapefruit and oranges. It is the most economically important postharvest disease of citrus in arid growing regions of the world[33,34] and usually causes losses from 20% to 30% during storage and marketing. In recent years, resistant strains of *Penicillium digitatum* were reported in packing houses in California and elsewhere.[35−37] With the spreading emergence of DMI resistance, there is a dire need of new, more selective and even more potent fungal CYP51 inhibitors for the treatment of pathogens of both human and plants. One practical solution is to investigate specifically the individual CYP51 of each pathogen species, respectively, followed by a delicate structure-based or site-directed mutation-based inhibitor design process. CYP51 from *Penicillium digitatum* (PD-CYP51) was, therefore, selected as a case study to examine whether our strategy is practicable.

To design new inhibitors with totally new molecular backbone, high selectivity, and potency targeting fungal CYP51s, the interaction mechanism between the active site of the specifically individual fungal CYP51 and its ligands need to be clearly elucidated. To do that an accurate three-dimensional (3-D) structure of target enzyme is a prerequisite. However, the fungal CYP51 proteins, unlike the soluble bacterial CYP51, are all integral membrane proteins, making structural and biophysical characterization more challenging.[38] A X-ray crystallographic study of CYP51 from bacterium *Mycobacterium tuberculosis* (MT-CYP51) was reported in 2001,[39] which is the unique published CYP51 crystal structure up to now. Being evolutionarily distant, CYP51s from different phyla have low sequence similarity across biological kingdoms and contain only about forty-one conserved amino acid residues in the whole family.[41] Fifteen of these residues lie in the secondary structural elements of MT-CYP51 and were predicted to function as potential substrate recognition sites of the P450 family.[40] Many studies have shown that most of the conserved residues throughout the CYP51s family are essential for the P450 to function as a sterol 14α-demethylase, explaining why they have been conserved over hundreds of millions of years.[41] The high degree of structural conservation of the substrate-binding site, together with the complicated but similar catalytic cycle suggested that even with the low sequence identity, considerable structural conservation should be kept within the CYP51s family. As expected the secondary and supersecondary structural motifs, and characteristically hydrophobic and hydrophilic segments are highly conserved in the cytochrome P450 superfamily proteins.[40]

In the present case study, a homology modeling 3-D structure of PD-CYP51 was built by the CPHmodels method.[42,43] First, both the sequence and structure-conserved information were taken into account. Second, molecular dynamics simulating and molecular docking were carried out to further investigate the interaction information between the active site of PD-CYP51 and its ligands. Subsequently, structure-based inhibitor design was performed by the use of the Flex-Pharm/PMF/GOLD//FlexX/PMF/GOLD[44] molecular docking procedures to virtually filter out thirty potential hit compounds of PD-CYP51 from the SPECs database,[45] jointly evaluated by the binding modes, structural diversities, and chemical and physical characters of the scored compounds. Finally via a series of bioaffinity arrays at enzyme level and on *Penicillium digitatum* in vitro, seven hit compounds with new structural scaffold and potent inhibitory activity were selected out for the further structural modification or functional group alteration in the future.

MATERIALS AND METHODS

Homology Modeling. A detailed investigation of the sequence and structure information of target enzyme and the interaction mechanism between the active site of enzyme and its ligands play a crucial role in designing and developing highly potent enzyme−inhibitors. Most of the fungal CYP51 proteins, however, are integral membrane proteins, which make structural and biophysical characterization more challenging. In this case the homology modeling is an alternative tool to generate the 3-D structure of target PD-CYP51 using the X-ray crystallographic structural information of MT-CYP51[39] (PDB 1e9x) as template, which was the unique crystallographic structure in CYP51s family reported hitherto.

However, the sequence identity between the PD-CYP51 and MT-CYP51 is low, up to 25.6% (Figure S1 of the Supporting Information). A reliable homology modeling 3-D structure of PD-CYP51 might not be obtained by a direct homology modeling method based upon the only use of the lower sequence similarity, without the supporting of other structural information. Fortunately, most of the secondary and supersecondary structural motifs, characteristically hydrophobic and hydrophilic segments, the regions of the sequence containing the heme binding site, the oxygen binding site, and the site of interactions with redox partners are highly conserved in cytochrome P450 superfamily.[46] In this case, the accuracy of the homology modeling 3-D structure can be improved by taking into account further structural conservation information in addition to the information of sequence alignment. In the present study, CPHmodels 2.0 Server (an automated homology modeling server, http://www.cbs.dtu.dk/services/CPHmodels/) has been employed to build the homology modeling 3-D structure of target PD-CYP51, which is well documented elsewhere[43] combining utilization of sequence, structural, and functional information. The template recognition is based on profile−profile alignment guided by secondary structure and exposure predictions in CPHmodels Sever. The accurate template determination and sequence alignment algorithm will be able to enhance the reliability of the 3-D structure of homology modeling in this case study.

All hydrogen atoms were subsequently added to the unoccupied valence of heavy atoms of homology modeling PC-CYP51 at the neutral state using the BIOPOLYMER module of SYBYL 7.0 program package.[47]

Molecular Dynamics Simulating. The preceding homology modeling 3-D structure of PD-CYP51 was further subjected to a molecular dynamic (MD) study using the SANDER module of the AMBER 8.0 package[48] to reduce steric clashes and obtain converged 3-D modeling structure of PD-CYP51. The leaprc.ff99 force field parameters were loaded for the PD-CYP51 enzyme system, and a set of default parameters provided by the AMBER 8.0 was adopted for the cofactor heme. The whole system was first neutralized by adding Cl^- anion and then solvated into an octahedral box of TIP3P water molecules,[49] which extended at least 10 Å from any given atom of enzyme system of interest.

The particle mesh Ewald method[50−52] for the long-range electrostatics, a 10 Å cutoff for nonbonding van der Waals interactions, and periodic boundary conditions were set up for the following MD simulations. All bonds involving hydrogen were constrained using the SHAKE algorithm.[53] Constant temperature and pressure (300 K, 1 atm) were maintained using the Berendsen coupling algorithm[54] with a time constant for heat bath coupling of 2 ps. A time step of 1 fs was used to integrate the dynamic equations of motion. In addition, the following equilibration protocol was employed before starting the production-run phase. First, all water molecules of the TIP3P box were minimized 3000 steps by steepest descent and 3000 steps by conjugate gradient, respectively, while holding the enzyme system frozen. Then whole system (enzyme plus water box) was minimized 4000 steps by Amber force field with releasing the whole system. Finally, the whole system was slowly heated from 10 to 300 K over 100 ps before MD simulation. Trajectories were recorded every 1 ps during the entire MD simulation process. An averaged structure of PD-CYP51 theoretical model was derived from the trajectories of the last converged 1000 ps and subjected to a subsequent minimization using Tripos force field[55] of SYBYL 7.0 with a rms gradient of 0.05 kcal/(mol·Å) to generate the final theoretically predictive 3-D modeling structure of PD-CYP51 for subsequent molecular docking and virtual screening, which was submitted to PROCHECK[56,57] for a further reliability check as well.

Docking-Based Virtual Screening. The region of the active site was generated as follows: the resultant modeling structure of PD-CYP51 and the X-ray crystallographic structure of the template MT-CYP51 (1e9x) were superposed each other, then the heme cofactor and the 4-phenyl-1H-imidazole (PIM) of 1e9x were merged into the corresponding site of the PD-CYP51 modeling. All atoms located within the range of 6.5 Å from any atom of PIM were selected into the so-called active site, and the corresponding amino acid residue was, therefore, involved into the active site if only one of its atoms was selected.

FlexX is a fast and automated docking method, which takes ligand's conformational flexibility into account during the docking process by an incremental fragment placing technique.[58,59] FlexX-Pharm enables pharmacophore-type constraints to be used in FlexX to guide ligand docking.[60] FlexX embodied in SYBYL 7.0 package was carried out first to explore the binding model of ligands in the active site and validate the molecular docking process for the specific PD-CYP51 system, then followed by a structure-based high throughput virtual screening out of SPECs database. The virtual screening strategy adopted in the present study principally consisted of one step of 2-D ligand-based searching in terms of Lipinski rules[61] and two steps of 3-D receptor−ligand binding mode-based molecular docking by Flex-Pharm/PMF/GOLD and FlexX/PMF/GOLD evaluations for the compounds out of SPECs database.

The CScore of SYBYL 7.0[47] uses four types of scoring functions such as GOLD,[62] PMF,[63] DOCK,[64] and ChemScore[65] to rank the affinity of ligands bound to the active site of a receptor. GOLD scoring function well considers a range of nonpolar and hydrophobic interactions between enzyme and its ligand.[62] PMF scoring function applies a knowledge-based approach to exploit structural information by prelearning the structural information of known protein−ligand complexes in the PDB, and then converts the structural information into Helmholtz free interaction energies of protein−ligand,[63] which enabled PMF to be more sensitive to the experimental binding modes than other scoring functions. DOCK scoring function uses only the charge and van der Waals interactions between the protein and the ligand,[64] and ChemScore scoring function includes terms for hydrogen bonding, rotational entropy, and an intercept term.[65] Since the specificity of binding site of ligands of CYP51 is highly associated with the van der Waals (including $\pi-\pi$) interaction and hydrophobic character of residues (Ala108, Phe120, Met304, Ala305, Ile371, and Phe501), PMF and GOLD scoring functions were, therefore, jointly utilized in this virtual screening study to improve the quality of scoring. Specifically, FlexX/PMF was used first to get a proper binding mode of each screening compound, and subsequently FlexX/GOLD was used to calculate a more reliable estimation of binding energy. The FlexX/PMF/GOLD methodology was tested on cytochrome P450 3A4 substrates and inhibitors, and its effectiveness was demonstrated elsewhere.[43] Other default parameters in the FlexX module were adopted in the calculations of molecular docking and virtual screening. All calculations were performed on a CCNUGrid-based computational environment (CCNUGrid website http://202.114.32.71:8090/ccnu/chem/platform.xml).

Bioaffinity Testing. To evaluate the inhibitory activity of hit compounds virtually selected out in the present study, the binding constants (K_d) of hit compounds were determined at the PD-CYP51 recombinant protein level, together with the half maximal effective concentrations (EC_{50}) of hit compounds were measured on *Penicillium digitatum* in vitro.

The clone, expression, and purification of PD-CYP51 recombinant protein, as well as a build-up of bioaffinity testing system in vitro were carried out as previously reported.[66] Spectroscopic binding (K_d) assays were repeated three times in 100 mM potassium phosphate buffer at 25 °C by difference UV spectroscopy using S-3100 spectrophotometer (Sinco Co. Ltd.). The binding of a ligand to P450 elicits two major types of spectral changes:[17] type I, characteristic of substrate binding, with a broad spectral peak in the region of 370−390 nm and a trough in the region of 400−450 nm and type II, characteristic of inhibitor binding, with a broad spectral peak in the region of 400−450 nm and a trough in the region of 370−390 nm. The absorption spectral profile changes were dependent on ligands concentration, which enable us to evaluate the binding affinity of ligands to the heme iron in the active site. K_d values were calculated by nonlinear regression analysis using the equation $\Delta A=\Delta A_{max}[I]/(K_d + [I])$, where ΔA is the peak absorbance difference, ΔA_{max} is the difference in absorption at saturation, and [I] is the inhibitor or ligand concentration.[67] The new hit compounds reported in the present binding assays were purchased from SPECs,[44] and commercial control triadimefon was purchased from Chemical Company of Limin (Yancheng, China). The purity of all the purchased compounds is HPLC ≥ 95%.

Growth inhibition tests for the ten hit compounds well-performed at enzyme level and commercial control triadimefon on *Penicillium digitatum* in vitro were further carried out by using the culture medium treated by mycelial of 5

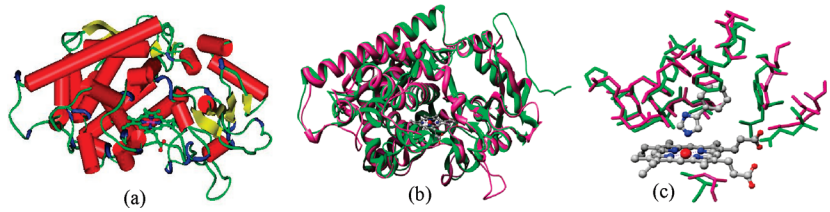

Figure 1. (a) Homology modeling 3-D structure of PD-CYP51 using PDB code of 1e9x as template. (b) Schematic for the superposition of MT-CYP51 template and the PD-CYP51 modeling 3-D structure by CPHmodels. Pink ribbon denotes the target protein, while green ribbon MT-CYP51 template in entire backbone. (c) The active site with ligand PIM for both template and target CYP51s.

mm diameter and a series of concentration of testing compounds, respectively, in Petri dishes of 8.5 cm diameter as reported by Yigit and coauthors.[68]

RESULTS AND DISCUSSION

Homology Modeling and Dynamics Simulating. The homology modeling of PD-CYP51 was reported by using the Fugue module of SYBYL 7.0 in the preceding study;[66] however, the whole protein chain was cut into two chains in the subsequent molecular dynamics simulation. To avoid the problem mentioned-above, the CPHmodels method was, therefore, chosen to rebuild the current homology modeling 3-D structure of PD-CYP51 (Figure 1a). As mentioned above, structure-based sequence profiles and folds recognition methods that combine sequence, structural, and functional information were involved into CPHmodels 2.0 Server. The accuracy of the homology modeling 3-D structure of PD-CYP51 by CPHmodels might be, therefore, improved by taking into account further structural conservation information in addition to the information of sequence alignment. Figure 1b shows the superposition of the homology modeling 3-D structure of PD-CYP51 constructed by CPHmodels method with that of template MT-CYP51, the root-mean-square deviation (rmsd) of the backbones of the whole protein between them is 1.5 Å. As expected, the overall conformation of the PD-CYP51 homology modeling 3-D structure is very similar to that of template MT-CYP51. Especially the regions of the sequence containing the heme binding site, the oxygen binding site, and the site of interactions with redox partners are conserved, the residues of the substrate and heme cofactor binding sites are almost identical, as shown in Figure 1c.

The preceding homology modeling 3-D structure of PD-CYP51 by CPHmodels was solvated in an octahedral box of TIP3P water molecules, and a MD simulation undergoing 7500 ps was carried out subsequently by using the SANDER module of the AMBER 8.0 package. The RMSDs of the geometric coordinates of C_α, C, and N atoms of both the entire enzyme backbone (black line in Figure 2) and the conserved amino acid residues involved in the active site (red line in Figure 2) between the simulated trajectories and the initial structure of the PD-CYP51model were calculated, respectively, over the simulation time by using the PTRAJ module of AMBER 8.0 and illustrated in Figure 2. The evolution of black line in Figure 2 showed that the whole system arrived at a convergence region of conformations after around 4500 ps of MD simulation at constant temperature and pressure. The evolution of red line in Figure 2 showed that the conserved amino acid residues of interest rapidly arrived at a dynamic convergence with the rmsd around 1.5−2.0 Å.

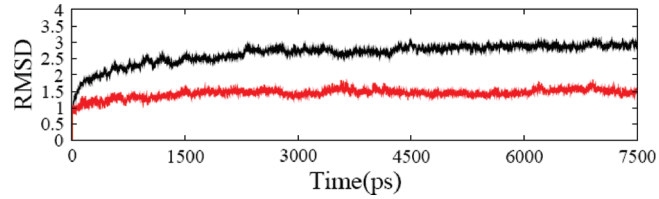

Figure 2. Plots of the root-mean-square deviation (rmsd, in Å) versus the MD simulation time in the MD simulated PD-CYP51 modeling trajectories. The black line represents the rmsd of Cα, C, and N atoms of the entire enzyme between the simulated trajectories and the initial structure of the PD-CYP51model. The red line represents the rmsd of Cα, C, and N atoms of the conserved amino acid residues between the simulated trajectories and the initial structure.

An averaged structure of PD-CYP51 theoretical model was derived from the trajectories of the last converged 1000 ps and subjected to a subsequent minimization using Tripos force field of SYBYL 7.0 with a rms gradient of 0.05 kcal/(mol Å) to generate the final theoretically predictive 3-D modeling structure of PD-CYP51 for subsequent molecular docking and virtual screening. The resultant 3-D modeling structure of the PD-CYP51 was further checked by PROCHECK method (illustrated in Figure S2, Supporting Information), and the results show that 76.7% of the residues were distributed in the most favored regions, 22.1% in the additional allowed regions, 0.7% in the generously allowed regions, and only 0.5% in the disallowed regions, respectively. This Ramachandran plots[69] (Figure S2, Supporting Information) checked results implied that the ultimate modeling 3-D structure of PD-CYP51 was most likely reliable.

Docking-Based Virtual Screening. First, to validate the reliability of the molecular docking methodology (FlexX/PMF/GOLD) adopted herein, the ligand PIM in the X-ray crystallographic structure of 1e9x was taken as a testing molecule. The initial geometric parameters of PIM backbone was extracted out of 1e9x, adding hydrogen atoms and subsequently submitted to a minimization by using the Tripos force field, and then PIM was docked back into the active site of 1e9x with the FlexX/PMF/GOLD method. The molecular docking results revealed that the binding mode of PIM obtained by FlexX/PMF/GOLD was almost identical to that of 1e9x crystal complex with rmsd 0.52 Å (as illustrated in Figure 3a). With the same molecular docking procedure the commercial DMI triadimefon (molecular formula shown in Table 1) was also docked into the active site of PD-CYP51 modeling (Figure 3b), which showed that the triazole N-1 hydrophobic group of triadimefon interacted with the hydrophobic or π-conjugated amino acid residues Phe120, Phe501, and Tyr112 of the substrate binding site. The distance between the coordinated nitrogen atom (N-3)

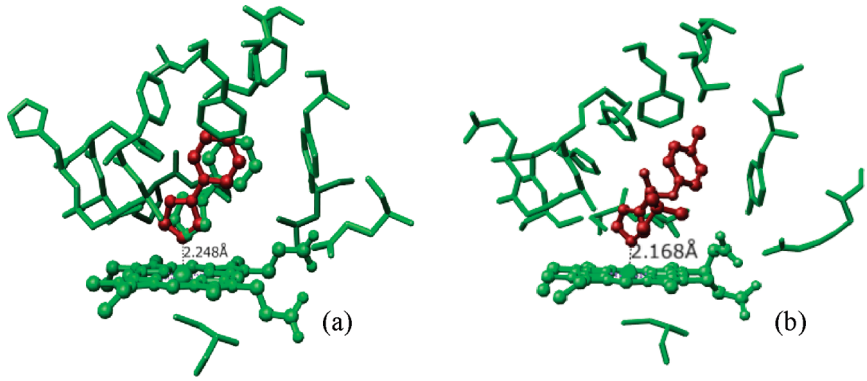

Figure 3. Schematic for the validation of molecular docking procedures of FlexX/PMF/GOLD. (a) Docking conformation (red) versus crystal binding conformation for the ligand PIM in the active site of MT-CYP51. (b) Docking conformation of triadimefon (red) in the active site of PD-CYP51 homology modeling.

Table 1. Binding Constants (K_d Values) at PD-CYP51 Enzyme Level As Well As EC_{50} Values for *P. digitatum* in Vitro

HIT COMPOUNDS ID	K_d (μM)	EC_{50} (ppm)
1	0.34 ± 0.55	38.86 ± 1.01
6	0.52 ± 0.16	6.39 ± 1.03
7	0.28 ± 0.19	3.42 ± 1.04
8	0.65 ± 0.44	9.56 ± 1.00
9	0.54 ± 0.10	6.27 ± 1.02
10	0.06 ± 0.02	0.76 ± 1.02
11	0.06 ± 1.03	2.06 ± 1.04
21	0.18 ± 0.18	2.28 ± 1.22
25	0.09 ± 0.05	129.93 ± 1.00
26	0.08 ± 0.08	63.25 ± 1.06
Triadimefon	0.31 ± 0.04	1.69 ± 1.06

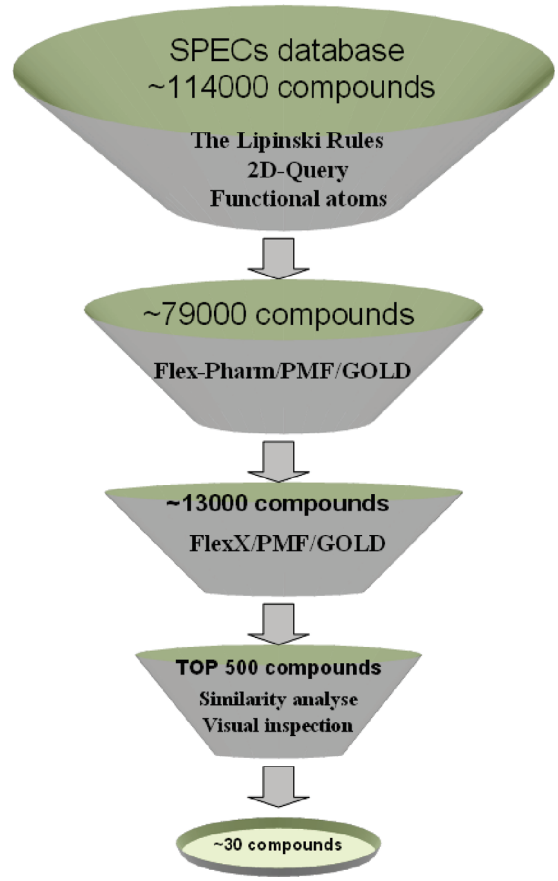

Figure 4. Schematic for the high throughput virtual screening protocol in the present study.

of triadimefon and the heme Fe atom is 2.2 Å, comparing with the corresponding counterpart 2.3 Å in the case of PIM of 1e9x crystal complex. Which implied that the binding mode of ligand obtained by the FlexX/PMF/GOLD method was most likely valid and to some extent lent partial credit to the current modeling 3-D structure of PD-CYP51 as well. Additionally the FlexX/PMF/GOLD methodology was tested on cytochrome P450 3A4 substrates and inhibitors and its effectiveness was demonstrated elsewhere.[43] Therefore, all the molecular docking processes in the later high throughput virtual screening protocol (illustrated in Figure 4) were performed by the Flex-Pharm/PMF//FlexX/PMF/GOLD procedures.

On the first step of 2-D ligand-based searching, the criteria in terms of the Lipinski rules (≤5 H-bond donors (no. of OH and NH groups), ≤10 H-bond acceptors (no. of O or N atoms), MW ≤500 Da, M log $P \leq 5$) was employed to preselect all the molecules out of the SPECs database. In addition, all the previous studies showed that all the ligands, including substrate and potent inhibitors must contain the atoms which can coordinate well with the heme Fe atom, therefore, all compounds which contain N, O, and S atoms will be sorted out for the further 3-D receptor−ligand binding mode-based virtual screening.

After above two processes around 79 000 compounds were obtained for the following Flex-Pharm/PMF/GOLD molecular docking-based screening. All the preselected compounds have been transformed from 2-D to 3-D by CONCORD module[70] of SYBYL7.0. Partial charges have been attributed to the atoms according to the method of Gasteiger_Hückel[71]

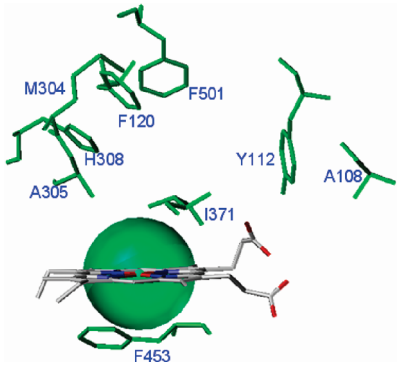

Figure 5. Schematic of the molecular docking cavity defined by Flex-Pharm constraints for virtual screening in the present study.

implemented in SYBYL 7.0. A proper virtual screening cavity was generated in terms of the active site of the resultant 3-D modeling structure of PD-CYP51, dominantly including heme, a series of hydrophobic amino acid residues Ala108, Phe120, Met304, Ala305, Ile371, Phe501, and several hydrophilic residues (illustrated in Figure 5). The most important Flex-Pharm constraint[60] is a spatial constraint defined by the distance to the heme Fe atom within 3.0 Å, a green sphere region shown in Figure 5, which was set as essential while other conserved residues were set as optional pharmacophore constraints since the native substrate coordinated well with the heme iron. Under this Flex-Pharm constraints only if the compound was docked into the cavity by Flex-Pharm/PMF with at least one N, O, or S atom within the green sphere region it were selected out immediately for a further judgment by scoring functional GOLD.

After the preceding Flex-Pharm/PMF/GOLD processes, 13 000 compounds were primitively selected out. A set of nonconstraints molecular docking processes, FlexX/PMF/GOLD, was subsequently performed in the same cavity to re-evaluate receptor−ligands binding interactions and cross-validate the binding modes, providing another set of FlexX scoring distribution of the selected compounds. The top 500 compounds in both of FlexX and Flex-Pharm scoring distribution were selected out for further comparison analysis. Some compounds have similar backbone and therefore were collected into one category, and we selected out the "best" one among them by jointly considering GOLD scoring, docked conformation, logP value and so forth of each compound. To do so, the representative thirty potential hit compounds were selected out by jointly using the GOLD score, binding mode, structural diversity, chemical and physical character for further bioaffinity testing at enzyme level and on *Penicillium digitatum* in vitro.

Bioaffinity Testing. UV−visible absorption spectroscopy provides a fast and accurate method for the determination of the binding constants (K_d) of ligands (substrate and inhibitors) to CYP51s. The lower the value of K_d, the greater the affinity of the enzyme for enzyme−inhibitor complex formation. The recombinant protein PD-CYP51 expressed in *Escherichia coli* revealed a typical absorption spectrum of reduced heme Fe(II)−CO with a Soret peak at around 449 nm and the oxidized state with a maximum at around 428 nm (as shown in Figure S3, Supporting Information).

To evaluate the inhibitory activity of hit compounds virtually selected out in the present study, a commercial azole-type DMI fungicide, triadimefon, was used as control array. Hit compounds obtained in this study, together with triadimefon were dissolved in dimethyl sulfoxide (DMSO), which never constituted more than 0.5% of the final sample volume. The well-performed hit compounds binding to the heme iron of recombinant protein PD-CYP51 gave rise to a typical type II spectrum with a broad spectral peak in the region of 390−410 nm and a trough in the region of 370−390 nm. Finally ten compounds out of thirty potential hit compounds with comparable binding affinities to that of the commercial triadimefon were selected out at enzyme level. The type II difference absorption spectra produced by the ten well-performed hit compounds, **1**, **6**, **7**, **8**, **9**, **10**, **11**, **21**, **25**, and **26**, and triadimefon in a series of concentration gradients (0.05, 0.10, 0.20, 0.40, 0.50, 0.75, 1.00, 2.00 μM) were collected into Figure S4, Supporting Information, together with the most probable binding modes for each hit compounds predicted by the present molecular modeling. The corresponding chemical structures, binding constants (K_d values) of the ten hits and commercial control were summarized in Table 1.

To further determine the effects of the preceding hit compounds on the mycelial growth and spore germination, one mycelial disk of 5 mm diameter was aseptically inoculated into the center of the Petri plate filled with potato dextrose agar (PDA) which was presoaked into a series of concentration gradients (3.125, 6.25, 12.5, 25.0, 50.0 ppm) of compounds of interest, together with blank control. After incubation for five days at 25 °C the diameters of fungal colonies were measured. Each assay was designated as three copies. Data were dealt with standard statistic analysis to obtain EC_{50} values of the corresponding compounds of interest, which were summarized into Table 1. It is clear from Table 1 that hit compounds **6**, **7**, **8**, **9**, **10**, **11**, and **21** have the same scale order of EC_{50} (ppm) values as that of triadimefon. Hit compounds **25**, **26**, and **1** have greater EC_{50} values than that of triadimenfon, albeit hits **25** and **26** have lower K_d values. There exists a discrepancy between the spectroscopic K_d values and EC_{50} values, which shows again that the binding constant does not accurately estimate inhibitory activity.[72] Therefore, a determination of EC_{50} assay is necessary in this study to be an auxiliary tool in evaluating the inhibitory potency of inhibitor.

The most probable binding modes for each hit compounds predicted in this study were illustrated in the Figure S4 of Supporting Information. The binding mode of hit compound Hit-7 was, as an example, further analyzed as follows. In Figure S4, Supporting Information, Hit-7 was illustrated in the form of ball-and-stick (yellow for sulfur atom, blue for nitrogen atom, red for oxygen atom, and gray for carbon atom), the amino acid residues of the active site were shown in green sticks, and the heme was depicted by sticks (gray for carbon atom, blue for nitrogen atom, and red for oxygen atom) and red ball for Fe atom. The distance between the S atom of Hit-7 and the Fe atom of heme is 2.9 Å; therefore, the S atom was predicted to coordinate well with the heme iron in the present docking study. N atom of the Hit-7 was predicted to interact with His308 via a hydrogen bond. Hydrophobic methyl phenoxide-like part of Hit-7 was predicted to locate into the cavity consisting of the hydrophobic residues Ala108, Phe120, Met304, Ala305, Ile371, and Phe501.

The best known DMI fungicides are the azole inhibitors, which mimic the structure of lanosterol, a key fungal sterol,

and possess an triazole[21−26] or imidazole[72−74] ring anchored at the heme iron of CYP51 through a nitrogen atom as the sixth coordination site to inactivate enzyme function. In those DMI fungicides, which do not contain an azole ring, an azole nitrogen-like atom should be available which serves a similar function. In the present virtual screening study, hit compounds 1, 6 belong to the common imidazole and triazole type compounds, however, hit compounds **7**, **8**, **9**, **10**, **11**, **21**, **25**, and **26** are not traditional azole-type compounds, which were most likely useful as new lead compounds of first generation with totally different molecular backbone from that of azoles.

CONCLUSION

Resistance to azoles is an emerging greater and greater challenge in controlling fungal pathogens of plants and human. One practical solution presented herein is to investigate specifically the individual CYP51 of each pathogen species, respectively, followed by a delicate structure-based inhibitor design to find more selective and higher potent novel fungicides targeting CYP51. As a demonstration, PD-CYP51 was selected as a case study to check whether the protocol of methodologies employed in the present study does work.

In this study, a homology modeling 3-D structure of PD-CYP51 was generated by CPHmodels, in which the accuracy of the homology modeling could be improved by taking into account further structural conservation information, using MT-CYP51 as the template. Interaction mechanism between the active site of PD-CYP51 and its ligands were further investigated by molecular dynamics simulating and molecular docking. With the effective docking process and interaction analysis information, structure-based high throughput virtual screening was performed to pick out the new potential inhibiting compounds from SPECs database by jointly using FlexX/PMF/GOLD and Flex-Pharm/PMF/GOLD methods. The representative thirty potential hit compounds were selected out by jointly using the GOLD score, binding mode, structural diversity, chemical and physical character for further bioaffinity testing. Finally the seven new hit compounds with comparable inhibitory activities to that of the commercial fungicide triadimefon were validated by a combining determination of K_d and EC_{50} values, which lends partial credit to the quality of molecular modeling strategy presented in this study. The positive results indicated that all modeling strategies and virtual screening processes presented in the current study most like to be an encouraging way in search of new lead compounds with brand-new molecular backbone for the specifically individual fungal CYP51s of both plants and human pathogens in the future.

ACKNOWLEDGMENT

This work was supported by the National Basic Research Program of China (Nos. 2010CB126103, 2007CB116302), the Natural Science Foundation of China (Nos. 20672041, 20873049, 20872044, 30900054, and 30771429), the Program for New Century Excellent Talents in University of China (NCET-06-0673), China National Technology Platform (No.2005DKA64001), and grant of State Key Laboratory of Physical Chemistry of Solid Surfaces at Xiamen University, China.

Supporting Information Available: Figures showing the sequence alignments on MT-CYP51 template and PD-CYP51 target enzymes, schematic for the quality of the modeling, typical CO-reduced, CO-oxidized binding spectrum, and PD_CYP51 type II binding spectra. This material is available free of charge via the Internet at http://pubs.acs.org.

REFERENCES AND NOTES

(1) Yoshida, Y. Sterol biosynthesis. In *Cytochrome P-450*, 2nd ed.; Omura, T., Ishimura, Y., Fujii-Kuriyama, Y., Eds.; Kodansha: Tokyo, 1993; pp 93−101.
(2) Yoshida, Y.; Aoyama, Y.; Noshiro, M.; Gotoh, O. Sterol 14-demethylase P450 (CYP51) provides a breakthrough for the discussion on the evolution of cytochrome P450 gene superfamily. *Biochem. Biophys. Res. Commun.* **2000**, *273*, 799–804.
(3) Fischer, R. T.; Trzaskos, J. M.; Magolda, R. L.; Ko, S. S.; Brosz, C. S.; Larsen, B. Lanosterol 14α-methyl demethylase. Isolation and characterization of the third metabolically generated oxidative demethylation intermediate. *J. Biol. Chem.* **1991**, *266*, 6124–6132.
(4) Werck, R. D.; Hehn, A.; Didierjean, L. Cytochromes P450 for engineering herbicide tolerance. *Trends Plant Sci.* **2000**, *5*, 116–123.
(5) Sheehan, D. J.; Hitchcoch, C. A.; Sibley, C. M. Current and emerging azole antifungal agents. *Clin. Microbiol. Rev.* **1999**, *12*, 40–79.
(6) Lamb, D. C.; Kelly, D. E.; Kelly, S. L. Molecular aspects of azole antifungal action and resistance. *Drug Resis Updat.* **1999**, *2*, 390–402.
(7) Lamb, D. C.; Kelly, D. E.; Baldwin, B. C.; Kelly, S. L. Differential inhibition of human CYP3A4 and *Candida albicans* CYP51 with azole antifungal agents. *Chem. Biol. Interact.* **2000**, *125*, 165–175.
(8) Lamb, D. C.; Kelly, D. E.; Schunck, W. H.; Shyadehi, A. Z.; Aktar, M.; Lowe, D. J.; Baldwin, B. C.; Kelly, S. L. The mutation T315A in Candida albicans sterol 14α-demethylase causes reduced enzyme activity and fluconazole resistance through reduced affinity. *J. Biol. Chem.* **1997**, *272*, 5682–5688.
(9) Souter, A.; McLean, K. J.; Smith, W. E.; Munro, A. W. The genome sequence of *Mycobacterium tuberculosis* reveals cytochromes P450 as novel anti-TB drug targets. *J. Chem. Technol. Biotechnol.* **2000**, *75*, 933–941.
(10) Guardiola-Diaz, H. M.; Foster, L. A.; Mushrush, D.; Vaz, A. D. Azole-antifungal binding to a novel cytochrome P450 from Mycobacterium tuberculosis: implications for treatment of tuberculosis. *Biochem. Pharmacol.* **2001**, *61*, 1463–1470.
(11) Munro, A. W.; McLean, K. J.; Marshall, K. R.; Warman, A. J.; Lewis, G.; Roitel, O.; Sutcliffe, M. J.; Kemp, C. A.; Modi, S.; Scrutton, N. S.; Leys, D. Cytochromes P450: Novel drug targets in the war against multidrug-resistant *Mycobacterium tuberculosis*. *Biochem. Soc. Trans.* **2003**, *31*, 625–630.
(12) McLean, K. J.; Marshall, K. R.; Richmond, A.; Hunter, S. I.; Fowler, K.; Kieser, T.; Gurcha, S. S.; Besra, G. S.; Munro, A. W. Azole antifungals are potent inhibitors of cytochrome P450 mono-oxygenases and bacterial growth in mycobacteria and streptomycetes. *Microbiology.* **2002**, *148*, 2937–2949.
(13) Talbot, N. J.; Ebbole, D. J.; Hamer, J. E. Identification and characterization of MPG1, a gene involved in pathogenicity from the rice blast fungus *Magnaporthe grisea*. *Plant Cell.* **1993**, *5*, 1575–1590.
(14) Hamamoto, H.; Hasegawa, K.; Nakaune, R.; Lee, Y. J.; Makizumi, Y.; Akutsu, K.; Hibi, T. Tandem repeat of a transcriptional enhancer upstream of the sterol 14alpha-demethylase gene (CYP51) in *Penicillium digitatum*. *Appl. Environ. Microb.* **2000**, *66*, 3421–3426.
(15) Sun, Q. Y.; Cao, Y. B.; Xu, J. M.; Zhang, W. N.; Zhang, J.; Wu, Q. Y.; Zhang, D. Z.; Jiang, Y. Y. Synthesis and antifungal activity of novel triazole derivatives. *Chem. J. Chin. Univ.* **2007**, *28*, 1707–1709.
(16) Schiaffella, F.; Macchiarulo, A.; Milanese, L.; Vecchiarelli, A.; Costantino, G.; Pietrella, D.; Fringuelli, R. Design, synthesis, and microbiological evaluation of new *Candida albicans* CYP51 inhibitors. *J. Med. Chem.* **2005**, *48*, 7658–7666.
(17) Podust, L. M.; Von, K.; Jens, P.; Eddine, A. N.; Kim, Y. C.; Yermalitskaya, L. V.; Kuehne, R.; Ouellet, H.; Warrier, T.; Altekoster, M.; Lee, J. S.; Rademann, J.; Oschkinat, H.; Kaufmann, H. E.; Waterman, M. R. Small-molecule scaffolds for CYP51 inhibitors identified by high-throughput screening and defined by X-ray crystallography. *Antimicrob. Agents Chemother.* **2007**, *51*, 3915–3923.
(18) Chen, C. K.; Doyle, P. S.; Yermalitskaya, L. V.; Mackey, Z. B.; Ang Kenny, K. H.; McKerrow, J. H.; Podust, L. M. Trypanosoma cruzi CYP51 Inhibitor Derived from a Mycobacterium tuberculosis Screen Hit. *PLoS Neglected Trop. Dis.* **2009**, *3*, 372.
(19) Debeljak, N.; Fink, M.; Rozman, D. Many facets of mammalian lanosterol 14α-demethylase from the evolutionarily conserved cytochrome P450 family CYP51. *Arch. Biochem. Biophys.* **2003**, *409*, 159–171.

(20) Cools1, H. J.; Fraaije, B. A.; Kim, S. H.; Lucas, J. A. Impact of changes in the target P450 CYP51 enzyme associated with altered triazole sensitivity in fungal pathogens of cereal crops. *Biochem. Soc. Trans.* **2006**, *34*, 1219–1222.

(21) Van Cutsem, J. M.; Thienpont, D. Miconazole, a broad-spectrum antimycotic agent with antibacterial activity. *Chemotherapy* **1972**, *17*, 392–404.

(22) Polak, A. Oxiconazole, a new imidazole derivative. Evaluation of antifungal activity in vitro and in vivo. *Arzneim. Forsch.* **1982**, *32*, 17–24.

(23) Odds, F. C.; Milne, L. J.; Gentles, J. C.; Ball, E. H. The activity in vitro and in vivo of a new imidazole antifungal, ketoconazole. *J. Antimicrob. Chemother.* **1980**, *6*, 97–104.

(24) Tsukioka, T. Determination of the fungicide trycyclazole in river water, soil and animal samples. *Analyst* **1988**, *113*, 193–195.

(25) Rouchaud, J.; Moons, C.; Meyer, J. A. The products of metabolism of [14C] triadimefon in the grain and in the straw of ripe barley. *Bull. Environ. Contam. Toxicol.* **1981**, *27*, 543–550.

(26) Yoshida, Y.; Aoyama, Y.; Takano, H.; Kato, T. Stereo-selective interaction of enantiomers of diniconazole, a fungicide, with purified P-450/14DM from yeast. *Biochem. Biophys. Res. Commun.* **1986**, *137*, 513–519.

(27) Eckert, J. W.; Sievert, J. R.; Ratnayake, M. Reduction of imazalil effectiveness against citrus green mold in California packinghouses by resistant biotypes of *Penicillium digitatum*. *Plant Dis.* **1994**, *78*, 97–974.

(28) Lupetti, A.; Danesi, R.; Campa, M.; TaccaL, M. D.; Kelly, S. Molecular basis of resistance to azole antifungals. *Trends Mol. Med.* **2002**, *8*, 76–81.

(29) Marichal, P.; Bossche, V. V.; Odds, F. C.; Nobels, G.; Warnock, D. W.; Timmerman, V.; Broeckhoven, C. V.; Fay, S.; Larsen, P. M. Molecular biological characterization of an azole-resistant *Candida glabrata* isolate. *Antimicrob. Agents Chemother.* **1997**, *41*, 2229–2237.

(30) Schnabel, G.; Jones, A. L. The 14α-demethylase (*CYP51A*) gene is overexpressed in *Venturia inaequalis* strains resistant to myclobutanil. *Phytopathology.* **2001**, *91*, 102–110.

(31) De'lye, C.; Laigret, F.; Corio-Costet, M. F. A mutation in the 14α-demethylase gene of *Uncinula necator* that correlates with resistance to a sterol biosynthesis inhibitor. *Appl. Environ. Microbiol.* **1997**, *63*, 2966–2970.

(32) Delye, C.; Bousset, L.; Corio-Costet, M. F. PCR cloning and detection of point mutations in the eburicol 14α-demethylase (*CYP51*) gene from *Erysiphe graminis f. sp. hordei*, a "recalcitrant" fungus. *Curr. Genet.* **1998**, *34*, 399–403.

(33) Holmes, G. J.; Eckert, J. W. Sensitivity of *Penicillium digitatum* and *P. italicum* to postharvest citrus fungicides in California. *Phytopathology.* **1999**, *89*, 716–721.

(34) Cabello, H. F.; Taton, M.; Forthoffer, N.; Kahn, R.; Bak, S.; Rahier, A.; Werck, R. D. Optimized expression and catalytic properties of a wheat obtusifoliol 14α-demethylase (CYP51) expressed in yeast. Eur. *J. Biochem.* **1999**, *262*, 435–446.

(35) Jennifer, M.; Ghosoph, L. S.; Schmidt, D. A.; Margosan, Joseph, L. S. Imazalil resistance linked to a unique insertion sequence in the *PdCYP51* promoter region of *Penicillium digitatum*. *Postharvest Biol. Technol.* **2007**, *44*, 9–18.

(36) Holmes, G. J.; Eckert, J. W. Relative fitness of imazalil-resistant and sensitive biotypes of *Penicillium digitatum*. *Plant Dis.* **1995**, *79*, 1068–1073.

(37) Wild, B. L. Differential sensitivity of citrus green mould isolates (*Penicillium digitatum* Sacc.) to the fungicide imazalil. *N. Z. J. Crop Hortic. Sci.* **1994**, *22*, 167–171.

(38) Holtje, H. D.; Fattorusso, C. Construction of a model of the *Candida albicans* lanosterol 14-[alpha]-demethylase active site using the homology modelling technique. *Pharm. Acta Helv.* **1998**, *72*, 271–277.

(39) Podust, L. M.; Poulos, T. L.; Waterman, M. R. Crystal structure of cytochrome P450 14α-sterol demethylase (CYP51) from *Mycobacterium tuberculosis* in complex with azole inhibitors. *Proc. Natl. Acad. Sci. U. S. A.* **2001**, *98*, 3068–3073.

(40) Lepesheva, G. I.; Virus, C.; Waterman, M. R. Conservation in the CYP51 Family. Role of the B¢ Helix/BC Loop and Helices F and G in Enzymatic Function. *Biochemistry* **2003**, *42*, 9091–9101.

(41) Lepesheva, G. I.; Waterman, M. R. CYP51—The omnipotent P450. *Mol. Cell. Endocrinol.* **2004**, *215*, 165–170.

(42) Lund, O.; Frimand, K.; Gorodkin, J.; Bohr, H.; Bohr, J.; Hansen, J.; Brunak, S. Protein distance constraints predicted by neural networks and probability density functions. *Protein Eng.* **1997**, *10*, 1241–1248.

(43) Lund, O.; Nielsen, M.; Lundegaard, C.; Worning, P. CPHmodels 2.0: X3M a Computer Program to Extract 3D Models. Abstract at the CASP5 conference A102, 2002.

(44) György, M. K. A virtual high throughput screen for high affinity cytochrome P450cam substrates. Implications for in silico prediction of drug metabolism. *J. Comput.-Aided Mol. Des.* **2001**, *15*, 649–657.

(45) SPECs provides chemistry and chemistry related services that are required in drug discovery. 1987. http://www.specs.net.

(46) Ji, H. T.; Zhang, W. N.; Zhou, Y. J.; Zhang, M.; Zhu, J.; Song, Y. L.; Lü, J. G.; Zhu, J. A three-dimensional model of lanosterol 14α-demethylase of *Candida albicans* and its interaction with azole antifungals. *J. Med. Chem.* **2000**, *43*, 2493–2505.

(47) *SYBYL7.0*; Tripos Inc.: St. Louis, MO, 2003.

(48) Case, D. A.; Darden, T. A.; Cheatham, T. E., III.; Simmerling, C. L.; Wang, J.; Duke, R. E.; Luo, R.; Merz, K. M.; Wang, B.; Pearlman, D. A.; Crowley, M.; Brozell, S.; Tsui, V.; Gohlke, H.; Mongan, J.; Hornak, V.; Cui, G.; Beroza, P.; Schafmeister, C.; Caldwell, J. W.; Ross, W. S.; Kollman, P. A. *AMBER8*; University of California: San Francisco, CA, 2004.

(49) Jorgensen, W. L.; Chandrasekhar, J.; Madura, J.; Klein, M. L. Comparison of simple potential functions for simulating liquid water. *J. Chem. Phys.* **1983**, *79*, 926–935.

(50) Darden, T.; York, D. L. Pedersen, Particle mesh Ewald: An *N* log(*N*) method for Ewald sums in large system. *J. Chem. Phys.* **1993**, *98*, 10089–10092.

(51) Essmann, U.; Perera, L.; Berkowitz, M. L.; Darden, T.; Lee, H.; Pedersen, L. G. A smooth particle mesh Ewald method. *J. Chem. Phys.* **1995**, *103*, 8577–8593.

(52) Sagui C.; Darden, T. A. P3M and PME: a comparison of the two methods. In *Simulation and Theory of Electrostatic Interactions in Solution*, Pratt, L. R., Hummer, G., Eds.; American Institute of Physics: Melville, NY, 1999; pp 104−113.

(53) Ryckaert, J. P.; Ciccotti, G.; Berendsen, H. J. C. Numerical intergration of the Cartesian equations of motion of a system with constraints: Molecular synamics of *n*-alkanes. *J. Comput. Phys.* **1977**, *23*, 327–341.

(54) Berendsen, H. J. C.; Postma, J. P. M.; Van Gunsteren, W. F.; DiNola, A.; Haak, J. R. Molecular dynamics with coupling to an external bath. *J. Comput.Phys.* **1984**, *81*, 3684–3690.

(55) Clark, M.; Cramer, R. D., III.; Van Opdenbosch, N. Validation of the general purpose Tripose 5.2 force field. *J. Comput. Chem.* **1989**, *10*, 982–1012.

(56) Laskowski, R. A.; MacArthur, M. W.; Moss, D. S.; Thornton, J. M. PROCHECK: A program to check the stereochemical quality of protein structures. *J. Appl. Crystallogr.* **1993**, *26*, 283–291.

(57) Rullmann, J. A. C. *AQUA*; Utrecht University: Utrecht, The Netherlands, 1996.

(58) Rarey, M.; Kramer, B.; Lengauer, T.; Klebe, G. A Fast Flexible Docking Method Using an Incremental Construction Algorithm. *J. Mol. Biol.* **1996**, *261*, 470–489.

(59) Kramer, B.; Rarey, M.; Lengauer, T. Evaluation of the FlexX Incremental Construction Algorithm for Protein-Ligand Docking. *Proteins: Struct. Funct. Genet.* **1999**, *37*, 228–234.

(60) Hindle, S. A.; Rarey, M.; Buning, C.; Lengaue, T. Flexible docking under pharmacophore type constraints. *J. Comput. Aided Mol. Des.* **2002**, *16*, 129–149.

(61) Lipinski, C. A.; Lombardo, F.; Dominy, B. W.; Feeney, P. Experimental and computational approaches to estimate solubility and permeability in drug discovery and development settings. *J. Adv. Drug Delivery Rev.* **1997**, *23*, 3–25.

(62) Jones, G.; Willett, P.; Glen, R. C. Molecular recognition of receptor sites using a genetic algorithm with a description of desolvation. *J. Mol. Biol.* **1995**, *245*, 43–53.

(63) Muegge, I.; Martin, Y. C. A general and fast scoring function for protein−ligand interactions: A simplified potential approach. *J. Med. Chem.* **1999**, *42*, 791–804.

(64) Kuntz, I. D.; Blaney, J. M.; Oatley, S. J.; Langridge, R.; Ferrin, T. E. A geometric approach to macromolecule−ligand interactions. *J. Mol. Biol.* **1982**, *161*, 269–288.

(65) Eldridge, M. D.; Murray, C. W.; Auton, T. R.; Paolini, G. V.; Mee, R. P. Empirical scoring functions: I. The development of a fast empirical scoring function to estimate the binding affinity of ligands in receptor complexes. *J. Comput.-Aided Mol. Des.* **1997**, *11*, 425–445.

(66) Zhao, L.; Liu, D. L.; Zhang, Q. Y.; Zhang, S.; Wan, J.; Xiao, W. J. Expression and homology modeling of sterol 14α-demethylase from *Penicillium digitatum*. *FEMS Microbiol. Lett.* **2007**, *277*, 37–43.

(67) Rao, S.; Wilks, A.; Hamberg, M.; Ortiz de Montellano, P. R. The lipoxygenase activity of myoglobin. Oxidation of linoleic acid by the ferryl oxygen rather than protein radical. *J. Biol. Chem.* **1994**, *269*, 7210–7216.

(68) Yiğit, F.; özcan, M.; Akgül, A. Inhibitory effect of some spice essential oils on *Penicillium digitatum* causing postharvest rot in citrus. *Grasas Aceites* **2000**, *51*, 237–240.

(69) Morris, A. L.; MacArthur, M. W.; Hutchinson, E. G.; Thornton, J. M. Stereochemical quality of protein structure coordinates. *Proteins: Struct. Funct. Bioinf.* **1992**, *12*, 345–364.

(70) Rusinko, III. A.; Skell, J. M.; Balducci, R. et al. *CONCORD*; University of Texas and Tripos Associates: , Austin, TX and St Louis, MO, 1988.
(71) Gasteiger, J.; Marsili, M. Iterative partial equalization of orbital electronegativity—A rapid access to atomic charges. *Tetrahedron.* **1980**, *36*, 3219–3228.
(72) Verras, A.; Kuntz, I. D.; de Montellano, P. R. O. Computer-assisted design of selective imidazole inhibitors for cytochrome P450 enzymes. *J. Med. Chem.* **2004**, *47*, 3572–3579.
(73) Santo, R. D.; Tafi, A.; Costi, R.; Botta, M.; Artico, M.; Corelli, F.; Forte, M.; Caporuscio, F.; Angiolella, L.; Palamara, A. T. Antifungal Agents. 11. *N*-Substituted derivatives of 1-[(aryl)(4-aryl-1*H*-pyrrol-3-yl)methyl]-1*H*-imidazole: Synthesis, anti-candida activity, and QSAR studies. *J. Med. Chem.* **2005**, *48*, 5140–5153.
(74) Tafi, A.; Anastassopoulou, J.; Theophanides, T.; Botta, M.; Corelli, F.; Massa, S.; Artico, M.; Costi, R.; Santo, D. R.; Ragno, R. Molecular modeling of azole antifungal agents active against *Candida albicans*. 1. A comparative molecular field analysis study. *J. Med. Chem.* **1996**, *39*, 1227–1235.

CI900425T